Arch. Mech., 47, 3, pp. 577–599, Warszawa 1995

Shear band localization in saturated porous media (*)

B. A. SCHREFLER, C. E. MAJORANA
and L. SANAVIA (PADOVA)

A COMPUTATIONAL ANALYSIS of dynamic strain localization in multiphase solids is presented in this paper. The governing equations are obtained by means of averaging theories based on spatial averaging operators. Continuum wave propagation is used for the study of localization. The directions of localization are obtained by means of an eigenvalue analysis of the acoustic tensor. The investigation of the development of localized bands is carried out by means of a finite element code. The influence on localization of coupling between the constituents is studied. Several examples are shown.

Notation

s	solid phase,
f	fluid phase,
g	gaseous phase,
l	liquid phase,
$\mathbf{a}$	solid acceleration,
$\mathbf{a}^f$	fluid acceleration,
$\mathbf{b}$	body force vector,
$\mathbf{B}$	acoustic tensor,
c	acceleration wave speed,
C_s	specific moisture content,
$\mathbf{C}_T$	tangential constitutive tensor,
$\mathbf{D}$	Eulerian strain rate tensor,
d/dt	material time derivative with respect to the moving solid,
e	void ratio,
$f_{,i}$	$\partial f/\partial x_i$,
$f_{/i}$	$\partial f/\partial X_i$,
$\overline{g}$	gravity acceleration,
$\mathbf{E}$	deformation tensor,
$\mathbf{F}$	deformation gradient tensor,
$\mathbf{G}$	dynamic seepage matrix,
$\mathbf{H}$	permeability matrix,
$\mathbf{I}$	identity matrix 3×3,
K_s	solid grain bulk modulus,
K_T	overall skeleton bulk modulus,
K_l	fluid phase bulk modulus,
k_{rl}	liquid phase relative permeability,
$\mathbf{k}_{\alpha l}$	absolute permeability tensor,
$\mathbf{k}_l = \mathbf{k}_{\alpha l} k_{rl} \frac{\varrho_l \overline{g}}{\mu}$	permeability tensor,
$\mathbf{K}_T$	tangential stiffness tensor,

(*) Paper presented at 30th Polish Solid Mechanics Conference, Zakopane, September 5–9, 1994.

$\mathbf{K}_\sigma$ initial stress tensor,
$\mathbf{L}$ velocity gradient tensor,
$\mathbf{M}$ mass matrix,
$\mathbf{m}$ $[1\,1\,1\,0\,0\,0]^T$,
p_g gas pressure,
p_l water pressure,
$\mathbf{P}$ equivalent force vector,
$\mathbf{Q}$ coupled matrix,
$\mathbf{q}$ average relative water velocity,
$\mathbf{q}$ average relative gas velocity,
$\mathbf{R}$ rotation tensor,
$\mathbf{S}$ compressibility matrix,
S water saturation,
$(1-S)=S_g$ gas saturation,
t time variable,
$\mathbf{t}$ surface traction tensor,
$\mathbf{u}$ solid displacements,
$\mathbf{U}$ right stretch tensor,
$\mathbf{v}$ solid velocity,
$\mathbf{v}^f$ fluid velocity,
$\mathbf{v}^r$ relative velocity,
$\mathbf{V}$ left stretch tensor,
$\mathbf{W}$ spin tensor,
α Biot's coefficient,
β_1, β_2, Θ Newmark's parameters,
ε linear elastic strain tensor,
$\boldsymbol{\Theta}$ material rotation rate tensor,
η^i normal jump of the spatial velocity gradient,
μ liquid dynamic viscosity,
ϱ porous medium density,
ϱ_s solid grain density,
ϱ_l water density,
ϱ_g gas density,
σ Cauchy stress tensor,
$^J\dot{\sigma}$ Jaumann stress rate tensor,
σ'' effective stress tensor,
ϕ porosity.

Variable with overbar refers to the nodal values.

1. Introduction

GEOMATERIALS EXHIBIT, both in laboratory experiments and in field situations strain accumulations in well defined narrow zones. In such shear bands, material behaviour is inelastic, while the remaining zones are elastic, with infinitesimal strains. The triggering mechanisms for the formation of shear bands are inhomogeneities in the material and stress concentrations. Typical examples can be found in brittle geomaterials such as concrete and rocks, where progressive damage produces strain softening, or in soil as for instance in case of slope instability

or foundation failure. When the frictional properties of the material are more critical than the cohesive properties, we have Mode II (shear banding) dominated processes which may be simulated by plasticity models.

The analysis of strain localization is of importance in engineering practice because localization is a precursor to failure. In this work we present the theoretical framework of localization in geomaterials and the results of the first developments of computational investigations. Geomaterials are considered as multiphase materials in fully saturated conditions. The final aim however is to develop a model applicable both to fully saturated and partially saturated conditions.

It will be shown that the role of the fluid in localization is fundamental, since shear band formation preceding failure is affected by the interaction between solids and fluids, in terms of time sequence of band formation and the way of shear band development.

The topic of strain localization has been analysed in recent years by many authors, in particular in connection with single-phase solids [14]. The problem of dynamic localization in single phase solids has been investigated, e.g., by SLUYS [19]. Strain localization in multi-phase materials received less attention. Quasi-static cases were studied by RICE [16] and RUDNICKI [17] and dynamic cases by VARDOULAKIS [22]. A finite element analysis of dynamic strain localization of saturated porous media was first presented by LORET and PREVOST [10].

In the present paper we also use the dynamics of wave propagation [2] to investigate localization. Loret et Prevost applied a uniform axial compressive velocity jump along the top and bottom of a specimen, while Sluys used compressive impact loading. In both cases high frequency situations are studied where localization is initiated when the elastic loading wave hits the symmetry line (or immediately after). Here we show that dynamic localization may also be initiated by ramp loading which is more common in practical engineering situations. Localization starts here well after the first wave front hits the symmetry line but, as in the above cases, no weak element is needed to trigger off the formation of a shear band. This means that at least in fluid saturated media, propagating waves are not negligible even if a relatively small number of low frequencies govern the response.

The acoustic tensor is used as a search algorithm to determine the inclination angle of the shear band and as a check of the obtained numerical solution. This information may be used for mesh alignment. Coupling phenomena between solid skeleton and pore fluid are investigated in detail and the influence of permeability in fully saturated situations is pointed out. Pore pressure localization is also shown.

Since we aim to extend the model to partially saturated conditions, we treat the porous medium as a three-phase continuum, with the pores filled by water and air.

The fully saturated case, dealt with here, is only a subcase of the more general model. This model is explained next, following [12].

2. Mechanics of porous materials

2.1. Mathematical framework

2.1.1. Kinematics. The kinematics needed in the following is briefly recalled first.

Strain behaviour is locally defined by the deformation gradient tensor **F** [11, 12]. The polar decomposition theorem allows to express pure straining by the right stretch tensor **U** or the left stretch tensor **V**, while the rigid body rotation is described by the skew-symmetric tensor **R**:

$$F_{ij} = x_{i,j} = R_{ik}\, U_{kj} = V_{ik}\, R_{kj}\,. \tag{2.1}$$

The deformation process is described by the velocity gradient tensor **L**, which, referred to spatial coordinates, is given by

$$L_{ij} = v_{i,j} = \left(\dot{R}_{im}\, U_{mk} + R_{im}\, \dot{U}_{mk}\right)(R_{mk}\, U_{mj})^{-1}. \tag{2.2}$$

Its symmetric part is the Eulerian strain rate tensor **D**, related to pure straining component according to:

$$D_{ij} = \frac{1}{2}(L_{ij} + L_{ji}) = \frac{1}{2} R_{ik}\left[\dot{U}_{kn}\,(U_{nm})^{-1} + (U_{kn})^{-1}\,\dot{U}_{nm}\right] R_{jm}\,, \tag{2.3}$$

while its skew-symmetric component is the spin tensor **W**. This is commonly associated with the material rotation rate tensor $\Theta = \dot{\mathbf{R}}\mathbf{R}^T$ [13] (giving the angular velocity of the material [4]), even if it differs from it according to the following expression:

$$W_{ij} = \frac{1}{2}(L_{ij} - L_{ji}) = \dot{R}_{ik} R_{jk} + \frac{1}{2} R_{ik}\left[\dot{U}_{kn}(U_{nm})^{-1} - (U_{kn})^{-1}\,\dot{U}_{nm}\right] R_{jm}\,. \tag{2.4}$$

The approach adopted here to study the overall behaviour of multiphase media is an updated Lagrangian formulation, where the reference configuration is the last converged step. This description is properly Lagrangian only for the solid phase, while it is Eulerian in nature for the fluids: their relative flows are of importance here, hence their motion is referred to the actual configuration assumed by the solid skeleton.

The velocity and acceleration of each fluid particle can then be written with reference to the ones of the corresponding solid points, once the relative velocity, $\mathbf{v}^r$, is introduced. Assuming that kinematics variables not explicitly marked refer to the solid phase motion, we can write:

$$v_i^f = v_i + v_i^r\,, \qquad a_i^f = a_i + \frac{dv_i^r}{dt} + v_j^r (v_i + v_i^r)_{/j}\,, \tag{2.5}$$

where d/dt is the material time derivative with respect to the moving solid.

An average relative fluid velocity is obtained through averaging technique over a representative volume element dV. This velocity component is indicated by q_i for the liquid phase [18]:

$$v_i^{ls} = q_i = \frac{dV_f}{dV}\frac{dV_i}{dV_f}\langle v_i{}^r\rangle_l^l = \phi S\,\langle v_i{}^r\rangle_l^l \tag{2.6}$$

and by q_i for the gaseous phase.

$$v_i^{gs} = \mathrm{q}_i = \frac{dV_f}{dV}\frac{dV_g}{dV_f}\langle v_i^r\rangle_g^g = \phi(1-S)\langle v_i^r\rangle_g^g . \tag{2.7}$$

The averaging symbol $\langle\ \rangle$ is omitted in the following.

2.1.2. Balance equations. The macroscopic balance equations of mass and momentum are also obtained by means of systematic application of averaging procedures [7–9, 18] to the relevant balance equations of the constituents at microscopic level. The ensuing macroscopic balance equations coincide under appropriate assumptions with those of the classical mixture theories, integrated by the concept of volume fractions [6].

In the following, deviatoric stress components are not considered in fluids and compressive pore pressure is defined as positive. At the macroscopic level, the effects due to deviatoric stress components are accounted for through Darcy's law, by viscous drag forces exerted on the solid phase. Isothermal conditions and no phase changes are assumed and the phases are immiscible and chemically non-reacting.

The linear momentum balance equation for the whole mixture may be locally written in its Eulerian form [12] as:

$$\begin{aligned}\varrho b_i + \sigma_{ij/j} - \varrho a_i - \phi\varrho_f(a_i{}^f - a_i)\\ = \varrho b_i + \sigma_{ji/j} - \varrho a_i - \varrho_f\left[\phi\frac{dv_i{}^r}{dt} + q_j{}^f\left(v_{i/j} + v_{i/j}^r\right)\right] = 0.\end{aligned} \tag{2.8}$$

When this local condition is written for one phase alone, a specific term must be introduced to take into account the mechanical interactions occurring at the real interfaces with the other phases. These surfaces differ, in fact, from the boundary of the representative volume element over which the quantities are averaged. The external momentum supply represents the dissipative part of fluid-solid exchange,

$$S_i^{s\leftrightarrow f} = \phi\varrho_f a_i^f - \phi p_{f/i} - \phi\varrho_f b_i . \tag{2.9}$$

The mass conservation equation is introduced in its local form for the mixture water plus solid:

$$v_{i/i} + \frac{(1-\phi)}{\varrho_s}\frac{d\varrho_s}{dt} + \frac{\phi}{\varrho_l}\frac{d\varrho_l}{dt} + \frac{\phi}{S}\frac{dS}{dt} + \frac{q_{i/i}}{S} + \frac{q_i}{S\,\varrho_l}(\varrho_l)_{/i} = 0, \tag{2.10}$$

and for the mixture gas plus solid:

$$(2.11)\qquad v_{i/i} + \frac{(1-\phi)}{\varrho_s}\frac{d\varrho_s}{dt} + \frac{\phi}{\varrho_g}\frac{d\varrho_g}{dt} + \frac{\phi}{(1-S)}\frac{d(1-S)}{dt} + \frac{\mathrm{q}_{i/i}}{(1-S)} + \frac{\mathrm{q}_i}{(1-S)\varrho_g}(\varrho_g)_{/i} = 0.$$

According to the updated Lagrangian formulation applied, the convective components of acceleration must be considered only for the relative velocity of the fluids. Effective stress with the correction for multiphase flow, where saturations are used as weights, and with the further correction [24] for the deformability of the grains (with $\alpha = 1 - K_T/K_S$), is now introduced in the linear momentum balance equation. The equilibrium condition for the whole mixture can be written in its weak form as virtual velocity equation:

$$(2.12)\qquad \int_V \left[\sigma''_{ij} - \alpha\delta_{ij}(Sp_l + (1-S)p_g)\right] D_{ij}dV - \int_A f_i v_i\, dA - \int_V \varrho b_i v_i\, dV - \int_V \varrho\frac{dv_i}{dt}v_i\, dV + \int_V \phi\left[\varrho_l S\frac{d}{dt}\left(\frac{q_i}{\phi S}\right) + \varrho_g(1-S)\frac{d}{dt}\left(\frac{\mathrm{q}_i}{\phi(1-S)}\right)\right] v_i\, dV + \int_V \phi\left[\varrho_l q_j\left(\frac{q_i}{\phi S}\right)_{/j} + \varrho_g \mathrm{q}_j\left(\frac{\mathrm{q}_i}{\phi(1-S)}\right)_{/j}\right] v_i\, dV = 0.$$

The weak form of the continuity equations is obtained by integrating over the porous media volume the local conditions weighted with functions δp_α, which have continuity up to their first derivatives and satisfy the boundary conditions. The equation for water plus solid becomes [12]:

$$(2.13)\qquad \int_V \delta p_l \left\{\alpha S v_{i,i} + C_{ll}\dot{p}_l + C_{lg}\dot{p}_g + \left[\frac{C_{lg}}{(1-S)}(p_l - p_g) + \phi\right]\dot{S}\right\} dV + \int_V \delta p_l q_i \frac{(\varrho_l)_{/i}}{\varrho_l} dV + \int_V (\delta p_l)_{/i} q_i\, dV + \int_A \delta p_l q_i n_i\, dA = 0$$

and for the mixture gas plus solid:

$$(2.14)\qquad \int_V \delta p_g \left\{\alpha(1-S)v_{i,i} + C_{gg}\dot{p}_g + C_{lg}\dot{p}_g - \left[\frac{C_{lg}}{S}(p_g - p_l) + \phi\right]\dot{S}\right\} dV + \int_V \delta p_g \mathrm{q}_i \frac{(\varrho_g)_{/i}}{\varrho_g} dV + \int_V (\delta p_g)_{/i}\mathrm{q}_i\, dV + \int_A \delta p_g \mathrm{q}_i n_i\, dA = 0$$

(see Appendix for the coefficients C_{gg}, C_{lg} and C_{ll}).

2.1.3. Constitutive relationships. A hypoelastic constitutive relationship is here adopted. When dealing with large deformation effects, involving also large rotations, care must be taken in the material frame invariance of the law itself. This can be obtained by expressing the constitutive law as a function of objective fields, which here are chosen as the objective Eulerian strain rate **D** (Eq. (2.3)) and the associated objective stress rate measure defined by Jaumann [12], which is related to the Cauchy stress rate by the non-objective spin tensor, **W** (Eq. (2.4) through:

$$(2.15) \qquad {}^{J}\dot{\sigma}_{ij} = \dot{\sigma}_{ij} - \sigma_{ik}W_{jk} - \sigma_{mj}W_{im} = \dot{\sigma}_{ij} - {}^{R}\dot{\sigma}_{ij}$$
$$\text{with} \quad {}^{R}\sigma_{ij} = \dot{\sigma}_{ik}W_{jk} + \sigma_{jk}W_{ik}\,.$$

The constitutive law taking into account the modified effective stress principle mentioned above can thus be written in incremental form as:

$$(2.16) \qquad \dot{\sigma}_{ij} = C_{ijkl}D_{kl} - \alpha\delta_{ij}\left(S\,\dot{p}_l + (1-S)\,\dot{p}_g\right) + {}^{R}\dot{\sigma}_{ij}\,.$$

The Jaumann stress rate tensor can be properly used as a co-rotational measure associated with **D** in an updated Lagrangian approach with the strain increments kept small enough in each step of the analysis. In this hypothesis not only **D** gives a suitable description of the strain rate, but also **W** is an accurate approximation of the local angular velocity. This approach can also be used for elasto-plastic analyses, and leads to a good approximation in the hypothesis of small elastic components of deformation [12].

As far as the fluid phases are concerned, the constitutive equation governing the momentum exchange among different phases can be expressed as a function of average relative velocity, $\mathbf{q}^f$, once its frame invariance is proved. The latter variable depends on volume fractions, which are objective being scalar, and on the relative velocity, $\mathbf{v}^r$, which is also frame indifferent [12].

A thermodynamically consistent constitutive equation is then introduced for the dissipative part of fluid-solid exchange of momentum, which is related to fluid relative average velocity through the resistivity tensor $\Re^f$

$$(2.17) \qquad \mathcal{S}^{s\leftrightarrow f} = \phi\Re^f_{ij}q_j\,.$$

This relationship leads in fully saturated conditions to the generalised Darcy's law, which can be written in the following form:

$$(2.18) \qquad q_i = (k_{\alpha l})_{ij}\left[-(p_l)_{/j} + \varrho_l(b_j - a_j)\right].$$

For partially saturated conditions, the absolute permeability tensor $\mathbf{k}_{\alpha l}$ must be multiplied by the relative permeability k_{rl}, given as function of p_l [18]. A similar relationship has to be written for the gas phase.

The symmetric tensor $\mathbf{k}_{\alpha l}$, when the permeability is distributed in an anisotropic way, is updated according to $\mathbf{k}'_{\alpha l} = \mathbf{R}^T \mathbf{k}_{\alpha l} \mathbf{R}$.

In finite deformations this permeability tensor should be further updated if it is assumed to be a function of void ratio e, defined as the ratio between the void volume over the solid one. Being e_o in the initial configuration,

$$e_o = \frac{dV_o^l}{dV_o^s} = \frac{dV_o - dV_o^s}{dV_o^s} = \frac{\phi_o}{1-\phi_o} \tag{2.19}$$

we have in the actual configuration

$$e = \frac{\phi}{1-\phi} = \frac{dV}{dV_s} - 1 = \frac{dV}{dV_o}\frac{dV_o}{dV_o^s}\frac{dV_o^s}{dV^s} - 1 = J(1-e_o)J_s^{-1}. \tag{2.20}$$

Using an updated Lagrangian approach with time step increments small enough to have in each of them only a negligible contribution from the second order strain component, volume strain is satisfactorily approximated by the trace of the linear strain tensor. The current void ratio can then be evaluated by neglecting the specific contribution of proper grain deformation to the overall volume strain, which leads to

$$e = (1+e_o)(1+\operatorname{tr}\varepsilon) - 1 = e_o + (1+e_o)\operatorname{tr}\varepsilon. \tag{2.21}$$

2.1.4. Simplified governing equations. The numerical formulation actually implemented is developed assuming the gas phase at atmospheric pressure ($p_g = 0$).

Convective components of pressure and fluid density variation, which are seen to be not significant, are neglected and air density is assumed to be zero. In this case the mass balance of the mixture gas plus solid gives only the air flow and needs not to be considered.

Another simplification arises when acceleration frequencies are low, as is the case in earthquake motion: all the terms involving the relative component of fluid acceleration can then be ignored [24], being:

$$\left|a_i^l - a_i\right| = \left|\frac{d}{dt}\left(\frac{q_i}{\phi S}\right) + q_j\left(\frac{q_i}{\phi S}\right)_{/j}\right| \ll |a_i|. \tag{2.22}$$

This allows for reducing the primary variables to solid displacements and fluid pressure, and the final system to be solved consists of the momentum balance condition for the whole mixture and the continuity equation for the mixture water plus solid:

$$\int_V \sigma''_{ij} D_{ji}\, dV - \int_V \alpha\delta_{ij} S p_l D_{ji}\, dV - \int_A f_i v_i\, dA - \int_V \varrho b_i v_i\, dV - \int_V \varrho\, \dot{v}_i v_i\, dV = 0, \tag{2.23}$$

$$(2.24)\qquad \int_V \delta p_l \left(\alpha S v_{i,i} + \frac{1}{Q}\dot{p}_l\right) dV + \int_V (\delta p_l)_{/i} \left\{(k_{\alpha l})_{ij} \frac{k_{rl}}{\mu_l}\left[-(p_l)_{/j} + \varrho_l(b_j - a_j)\right]\right\} dV + \int_A \delta p_l q_i n_i \, dA = 0,$$

where, in the hypothesis of an isotropic medium, Darcy's law has been introduced in its generalised form.

The incremental solution of our problem can be obtained once the incremental form of the constitutive equation is given:

$$(2.25)\qquad d\sigma_{ij} = C_{ijkl} D_{kl}\, dt - \alpha \delta_{ij} S\, dp + d^R\sigma_{ij}$$

together with the saturation relationships

$$(2.26)\qquad p = S p_l \qquad S = S(p_l), \qquad k_{rl} = k_{rl}(p_l), \qquad C_S = \phi \frac{dS}{dp_l},$$

and the initial

$$(2.27)\qquad u_i = u_{0i}, \qquad \dot{u}_i = \dot{u}_{0i}, \qquad p = p_{l0},$$

and the boundary conditions are introduced:

$$(2.28)\qquad \begin{array}{lllll} \text{a) imposed displacements} & u_i = \bar{\bar{u}}_i & \text{on } \Gamma_u & \text{for } t \geq 0, \\ \text{b) imposed tractions} & t_i = \bar{\bar{t}}_i & \text{on } \Gamma_t & \text{for } t \geq 0, \\ \text{c) imposed pressures} & p_l = \bar{\bar{p}}_l & \text{on } \Gamma_{pl} & \text{for } t \geq 0, \\ \text{d) imposed flows} & q_i = \bar{\bar{q}}_i & \text{on } \Gamma_q & \text{for } t \geq 0. \end{array}$$

2.1.5. Spatial and time discretization. For a quantitative solution, Eqs. (2.23) and (2.24) are discretised in space by finite elements using Galerkin's procedure, and in time by Newmark's scheme [26]. The unknown field variables are expressed in the whole domain by global shape function matrices, $\mathbf{N}$ and $\mathbf{N}_p$, as functions of nodal value vectors $\bar{\mathbf{u}}$ and $\bar{\mathbf{p}}_l$:

$$(2.29)\qquad \mathbf{u} = \mathbf{N}\bar{\mathbf{u}}, \qquad p_l = \mathbf{N}_p \bar{\mathbf{p}}_l.$$

In the updated Lagrangian approach adopted, the strain operator, $\mathbf{B}_o$, which relates the strain rate vector with the vector of nodal velocities, is referred to the last known configuration

$$(2.30)\qquad \bar{\mathbf{D}} = \mathbf{B}_o \bar{\mathbf{v}}.$$

Once the coupling matrix $\mathbf{Q}$, the mass matrix $\mathbf{M}$ and the external load vector $\mathbf{f}^u$ are introduced (see Appendix), the equilibrium equation (2.23) can be written as

$$(2.31)\qquad \int_V \mathbf{B}_o^T \sigma''\, dV - \mathbf{Q}\bar{\mathbf{p}}_l + \mathbf{M}\ddot{\bar{\mathbf{u}}} = \mathbf{f}^u.$$

The continuity Eq. (2.24) becomes:

$$\mathbf{H}\,\bar{\mathbf{p}}_l + \mathbf{G}\,\ddot{\bar{\mathbf{u}}} + \mathbf{Q}^T\,\dot{\bar{\mathbf{u}}} + \mathbf{S}\,\dot{\bar{\mathbf{p}}}_l = \mathbf{f}^p, \tag{2.32}$$

where **H** is the permeability matrix, **G** the dynamic seepage matrix, **S** the compressibility matrix and $\mathbf{f}^p$ the flow vector (see Appendix). Since the effect of the dynamic seepage forcing term is negligible [23], the coupled system at time t_{n+1} is:

$$\begin{aligned} \mathbf{M}_{n+1}\,\ddot{\bar{\mathbf{u}}}_{n+1} + \bar{\mathbf{P}}_{n+1} - \mathbf{Q}_{n+1}\bar{\mathbf{p}}_{n+1} &= \mathbf{f}^u_{n+1}, \\ \mathbf{Q}_{n+1}\,\dot{\bar{\mathbf{u}}}_{n+1} + \mathbf{H}_{n+1}\bar{\mathbf{p}}_{n+1} + \mathbf{S}_{n+1}\,\dot{\bar{\mathbf{p}}}_{n+1} &= \mathbf{f}^p_{n+1}, \end{aligned} \tag{2.33}$$

where $\bar{\mathbf{P}}_{n+1}$ is the equivalent nodal force vector. The Newmark scheme adopted for time integration, with the lowest allowable order for each variable, permits to write the variables and their derivatives at t_{n+1} as functions of their values at t_n:

$$\begin{aligned} \dot{\bar{\mathbf{u}}}_{n+1} &= \dot{\bar{\mathbf{u}}}_n + \ddot{\bar{\mathbf{u}}}_n\,\Delta t + \beta_1 \Delta\ddot{\bar{\mathbf{u}}}\,\Delta t = \dot{\bar{\mathbf{u}}}^{\,p}_{n+1} + \beta_1\Delta\ddot{\bar{\mathbf{u}}}_n\,\Delta t, \\ \bar{\mathbf{u}}_{n+1} &= \bar{\mathbf{u}}_n + \dot{\bar{\mathbf{u}}}_n\Delta t + \frac{\ddot{\bar{\mathbf{u}}}_n\,\Delta t^2}{2} + \frac{\beta_2\Delta\ddot{\bar{\mathbf{u}}}_n\,\Delta t^2}{2} = \bar{\mathbf{u}}^p_{n+1} + \frac{\beta_2\Delta\ddot{\bar{\mathbf{u}}}_n\,\Delta t^2}{2}, \\ \bar{\mathbf{p}}_{n+1} &= \bar{\mathbf{p}}_n + \dot{\bar{\mathbf{p}}}_n\Delta t + \Theta\Delta\dot{\bar{\mathbf{p}}}_n\Delta t = \bar{\mathbf{p}}^p_{n+1} + \Theta\Delta\dot{\bar{\mathbf{p}}}_n\Delta t, \end{aligned} \tag{2.34}$$

where $\dot{\bar{\mathbf{u}}}^{\,p}_{n+1}$, $\bar{\mathbf{u}}^p_{n+1}$ and $\bar{\mathbf{p}}^p_{n+1}$ are predicted values from known parameters at time t_n.

Insertion of Eqs. (2.34) into (2.33) allows the coupled system to be written in the form

$$\begin{aligned} \Psi^u_{n+1} &= \mathbf{M}_{n+1}\Delta\ddot{\bar{\mathbf{u}}}_n + \bar{\mathbf{P}}_{n+1} - \mathbf{Q}_{n+1}\Theta\Delta t\Delta\dot{\bar{\mathbf{p}}}_n - \mathbf{F}^u_{n+1} = 0, \\ \Psi^p_{n+1} &= \mathbf{Q}^T_{n+1}\beta_1\Delta t\Delta\ddot{\bar{\mathbf{u}}}_n + \mathbf{H}_{n+1}\Theta\Delta t\Delta\dot{\bar{\mathbf{p}}}_n + \mathbf{S}_{n+1}\Delta\dot{\bar{\mathbf{p}}}_n - \mathbf{F}^p_{n+1} = 0. \end{aligned} \tag{2.35}$$

At the beginning of each time step $\bar{\mathbf{P}}_{n+1}$ must be evaluated by integration of the constitutive law, the stress field at the previous step being known. Relative permeability and specific capacity (Eq. (2.26)) must be updated as well as void ratio and absolute permeability.

The nonlinear coupled system (2.35) is solved by an iterative procedure. If a Newton–Raphson scheme is adopted to linearize the problem, the Jacobian matrix of transformation, **J**, at the i-th-iteration is:

$$\mathbf{J} = \left.\frac{\partial\Psi}{\partial x}\right|_{x=x_i} = \begin{pmatrix} \dfrac{\partial\Psi^u}{\partial\left(\Delta\ddot{\bar{\mathbf{u}}}\right)} & \dfrac{\partial\Psi^u}{\partial\left(\Delta\dot{\bar{\mathbf{p}}}\right)} \\ \dfrac{\partial\Psi^p}{\partial\left(\Delta\ddot{\bar{\mathbf{u}}}\right)} & \dfrac{\partial\Psi^p}{\partial\left(\Delta\dot{\bar{\mathbf{p}}}\right)} \end{pmatrix} = \begin{pmatrix} \mathbf{M} + \dfrac{1}{2}\mathbf{K}_T\beta_2\Delta t^2 & -\mathbf{Q}\Theta\Delta t \\ \mathbf{Q}^T\beta_1\Delta t & \mathbf{H}\Theta\Delta t + \mathbf{S} \end{pmatrix}. \tag{2.36}$$

The tangent stiffness matrix in Eq. (2.36) has been derived in [12] as

$$d\mathbf{P} = \int_V \left[\mathbf{B}_o^T \overline{\overline{\mathbf{C}}}\, \mathbf{B}_o + \mathbf{G}_r^T \hat{\sigma} \mathbf{G}_r\right] d\bar{\mathbf{u}}\, dV = (\mathbf{K} + \mathbf{K}_\sigma)\, d\bar{\mathbf{u}} = \mathbf{K}_T\, d\bar{\mathbf{u}}. \tag{2.37}$$

$\mathbf{K}_T$ is the sum of two terms: the matrix $\mathbf{K}$, corresponding to the linear elastic stiffness matrix, but referred to the constitutive matrix $\overline{\overline{\mathbf{C}}}$, modified by Cauchy stresses at time t, as:

$$\overline{\overline{\mathbf{C}}} = \mathbf{C} - \sigma_{d1} + \sigma_{d2} = \mathbf{C} - \sigma_d \tag{2.38}$$

and the initial stress matrix $\mathbf{K}_\sigma$, respectively equal to:

$$\mathbf{K} = \int_V \mathbf{B}_o^T \overline{\overline{\mathbf{C}}}\, \mathbf{B}_o\, dV, \qquad \mathbf{K}_\sigma = \int_V \mathbf{G}_r^T\, \hat{\sigma}\, \mathbf{G}_r\, dV. \tag{2.39}$$

Since the matrix σ_{d2} lacks in symmetry (see Appendix), $\mathbf{K}_T$ is also not symmetric, but this fact is usually negligible [13].

The system to be solved can then be written in the following form, which is symmetric provided the tangent stiffness matrix itself is symmetric:

$$\begin{pmatrix} \mathbf{M} + \frac{1}{2}\mathbf{K}_T \beta_2 \Delta t^2 & -\mathbf{Q}\Theta\Delta t \\ -\mathbf{Q}^T\Theta\Delta t & -\frac{\Theta}{\beta_1}(\mathbf{H}\Theta\Delta t + \mathbf{S}) \end{pmatrix} \begin{pmatrix} \Delta\, \ddot{\bar{\mathbf{u}}} \\ \Delta\, \dot{\mathbf{p}} \end{pmatrix} = \begin{pmatrix} -\Psi^u \\ -\frac{\Theta}{\beta_1}\Psi^p \end{pmatrix}. \tag{2.40}$$

Since the Newton–Raphson method requires the Jacobian matrix to be evaluated and inverted at each iteration, also other modified schemes are used to achieve convergence with less computational effort. In particular, the use of secant updates, like Davidon's and Broyden–Fletcher–Goldfarb–Shanno's (BFGS) methods are found advantageous in nonlinear analyses.

3. Dynamic localization theory in saturated porous solids

The finite strain localization theory is here based on the analysis of wave propagation in continuous solids. The first fundamental investigations on this subject are due to Duhem and Hadamard (1903). A presentation of the theory in general form and systematic literature references can be found in TRUESDELL and NOLL [20], TRUESDELL and TOUPIN [21] and in CHEN [2].

Let Σ be the wave front (here considered as a Riemannian manifold in motion, through which the acceleration and the velocity gradient can be discontinuous functions); $\mathbf{n}$ is the normal directed outward from the above manifold. Denoting

$$\eta^i = \operatorname{grad} \dot{\mathbf{x}}^i \tag{3.1}$$

the normal jump of the spatial velocity gradient of the i-phase along this manifold ($i = s, l$), Hadarmard's compatibility conditions can be written as

$$\left\| \dot{\mathbf{E}}^i \right\| = \frac{1}{2}\left(\eta^i \otimes \mathbf{n} + \mathbf{n} \otimes \eta^i\right), \tag{3.2}$$

$$\left\| \ddot{\mathbf{x}}^i \right\| = -c\eta^i, \tag{3.3}$$

where $\mathbf{E}^i$ is the deformation tensor of the i-phase, $\| \dots \|$ denotes the jump of the quantity inside the symbol, c represents the velocity of the manifold Σ with respect to the material frame of the analysed solid and $\otimes$ is, as usual, the dyadic or tensor product. Consequently, momentum equilibrium equations impose the condition

$$\| \dot{\sigma}^i \| \cdot \mathbf{n} = \varrho^i c^2 \eta^i. \tag{3.4}$$

Expressing the constitutive relationship in incremental form, LORET and PREVOST have shown in [10] that for the saturated case, c^2, squares of the wave propagation velocities coincide with the eigenvalues of the acoustic tensor $\mathbf{B}$, expressed by:

$$\mathbf{B} = \begin{pmatrix} \mathbf{B}^{ss} & \mathbf{B}^{sl} \\ (\mathbf{B}^{sl})^T & B^{ll} \end{pmatrix}, \tag{3.5}$$

where $B^{ll} = \dfrac{1}{\varrho^l}\dfrac{K}{\phi} > 0$ is a positive scalar quantity, $\mathbf{B}^{sl} = \dfrac{1}{\sqrt{\varrho^s \varrho^l}}\dfrac{1-\phi}{\phi} K_l \mathbf{n}$ is a vector and $\mathbf{B}^{ss} = \dfrac{1}{\varrho}\mathbf{n}\cdot\mathbf{A}^{ss}\cdot\mathbf{n}$ is a second order tensor containing the tensor of the solid moduli.

The hyperbolicity condition of the problem, implying an effective wave propagation, requires real values of the propagation velocity c. Consequently the eigenvalues of the tensor $\mathbf{B}$ must be real and positive. $\mathbf{B}$ inherits the symmetry properties of the solid moduli tensor and is hence symmetric for associative plasticity. In this case the eigenvalues are real and loss of hyperbolicity occurs in form of a stationary wave. In [10] it has been shown that the loss of hyperbolicity cannot occur for a positive plastic modulus. In case of non-associative plasticity $\mathbf{B}$ is no longer symmetric and loss of hyperbolicity may occur in form of flutter instability [10], where two square wave speeds become complex conjugate. In the following we assume associative plasticity and monitor the loss of hyperbolicity checking the sign of $\det \mathbf{B}$ in the Gauss points.

Developing the determinant of $\mathbf{B}$ matrix, it can be observed that the global result is related to the evolution of the constitutive parameters of the solid skeleton and the analysis of strain localization is reduced to the study of the sign of $\mathbf{n}\cdot\mathbf{A}'^{ss}\cdot\mathbf{n}$ [10].

In the two-dimensional case, $n_1 = \cos\vartheta$, $n_2 = \sin\vartheta$ hold; if one poses $x = \tan\vartheta$, the following expression is obtained

$$\det \mathbf{B}(\mathbf{n}) = P(x) = a_4x^4 + a_3x^3 + a_2x^2 + a_1x + a_0;$$

hence conditions for the onset of finite strain localization is transformed into a problem of searching the roots of a fourth degree polynomial or to find its minima by studying their signs (to find physically meaningful solutions).

4. Numerical examples

The two-dimensional domain of fully saturated porous material is discretised by means of isoparametric triangular or quadrilateral finite elements. Linear finite elements have been chosen because of their computational efficiency in nonlinear analysis and their low distortional characteristics.

The finite elements used for discretising the problem have not been intentionally oriented along particular lines (unbiased mesh).

The performed analyses show in particular:

i) the necessity of softening in the constitutive law (associative plasticity) to have shear band formation,

ii) the influence of permeability on band growth,

iii) particular patterns of stresses, pressures and strains with respect to the corresponding ones in hardening plasticity or elasticity,

iv) a weak mesh dependence of the results.

4.1. Quadrilateral sample

The onset and growth of localized bands in a soil sample of rectangular shape made of saturated material of dimensions 25×35 m are analysed (Fig. 1). The sample is subject to axial compression by means of uniformly distributed loads both on the upper and lower surfaces, as also indicated in Fig. 1.

The solid and fluid domains are not subject to any initial stress state (hence gravitational effects or hydrostatic pressures are not accounted for). In the fluid discretization the top and bottom surfaces are considered impermeable.

In the considered model, homogeneous and isotropic solid and fluid phases are taken into account. The constitutive relationship of the solid skeleton is of Mohr-Coulomb type, with a linear displacement-strain relationship.

It can be noted that plastic strains are concentrated in narrow bands of finite amplitude where high strain gradients occur (Fig. 2). In Fig. 3 localization directions are shown as found with the procedure based on the analysis of the acoustic tensor.

Figure 4 shows that in case of plasticity with hardening no band formation appears.

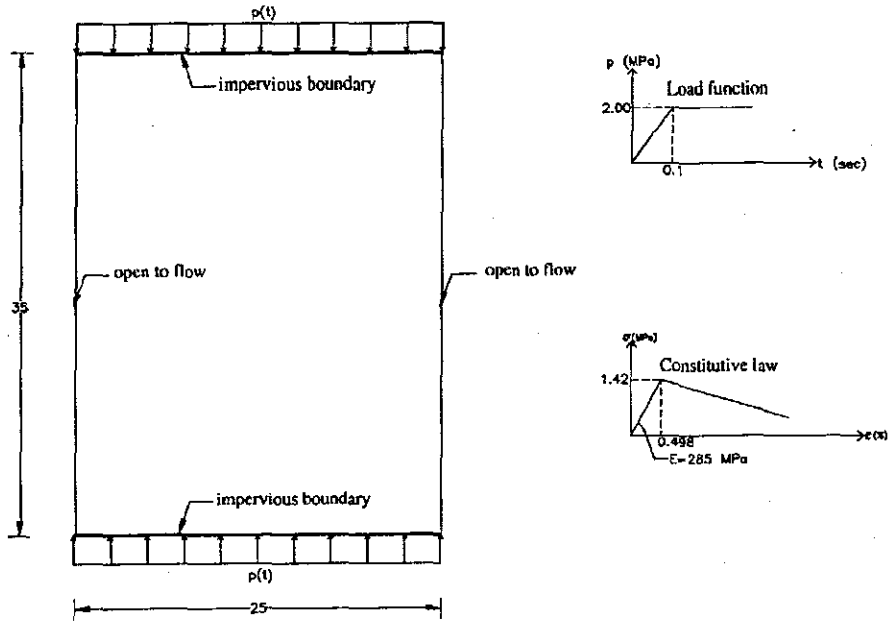

FIG. 1. Description of the geometrical and material characteristics of the reference example. Young's modulus $E = 285\,\text{MPa}$, Poisson's ratio $\nu = 0.4285$, solid grain density $\varrho_s = 2000\,\text{Kg/m}^3$, liquid density $\varrho_l = 1000\,\text{Kg/m}^3$, apparent cohesion $c_o = 1.42\,\text{MPa}$, hardening modulus $H = -40\,\text{MPa}$, angle of internal friction $\varphi = 20°$, volumetric liquid modulus $K_l = 200\,\text{MPa}$, volumetric solid modulus $K_s = 678\,\text{GPa}$, initial porosity $\phi_o = 0.2$.

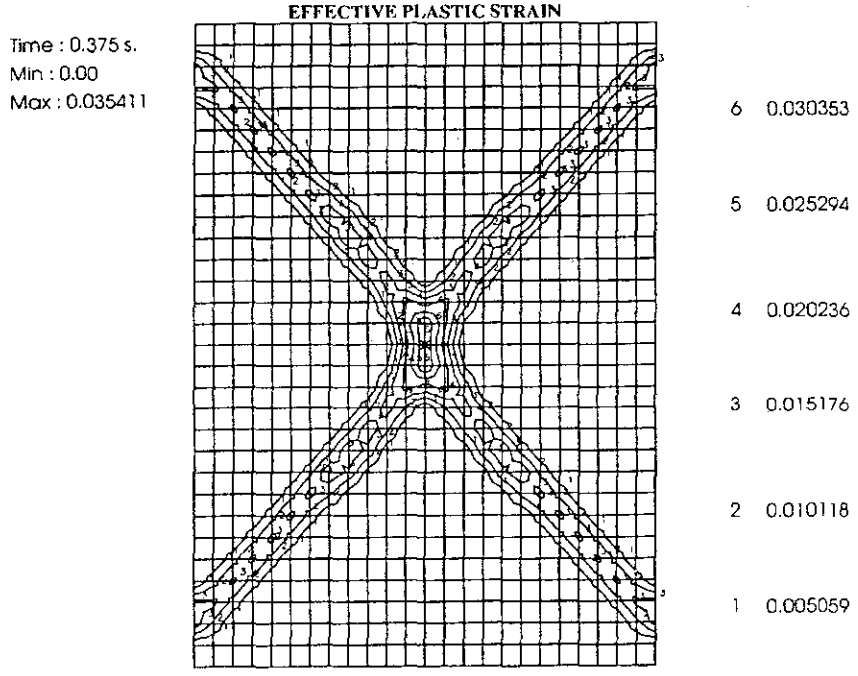

FIG. 2. Effective plastic strain at $t = 0.375\,\text{s}$ with a permeability of $0.25\,\text{m/s}$.

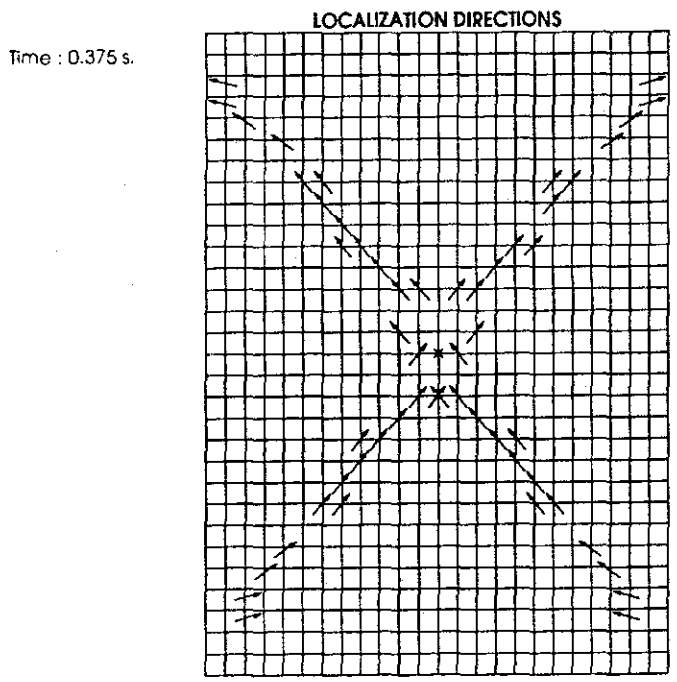

FIG. 3. Localization directions which follow from the analysis of the acoustic tensor.

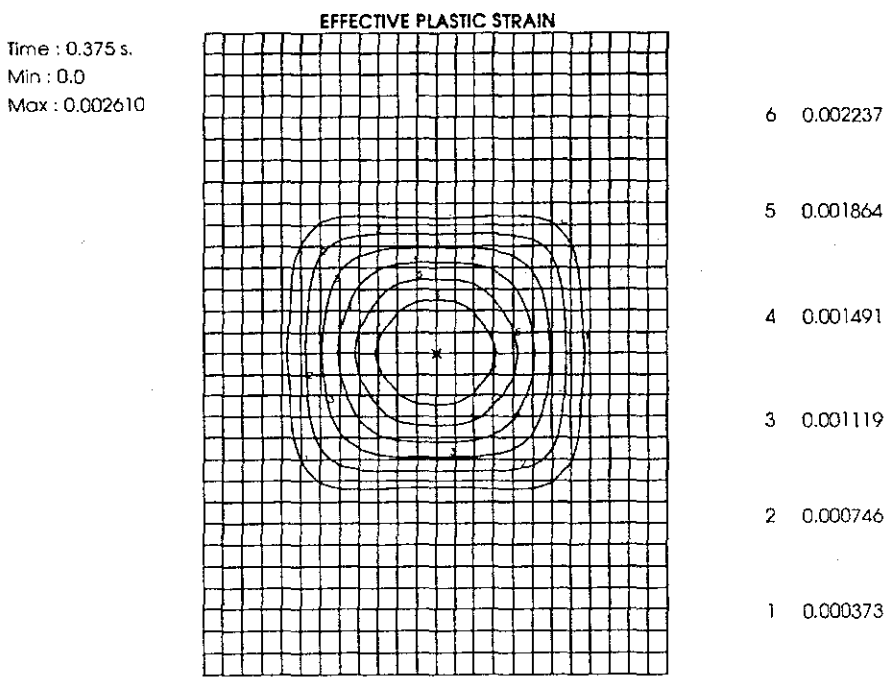

FIG. 4. Effective plastic strain at $t = 0.375$s in plasticity with hardening.

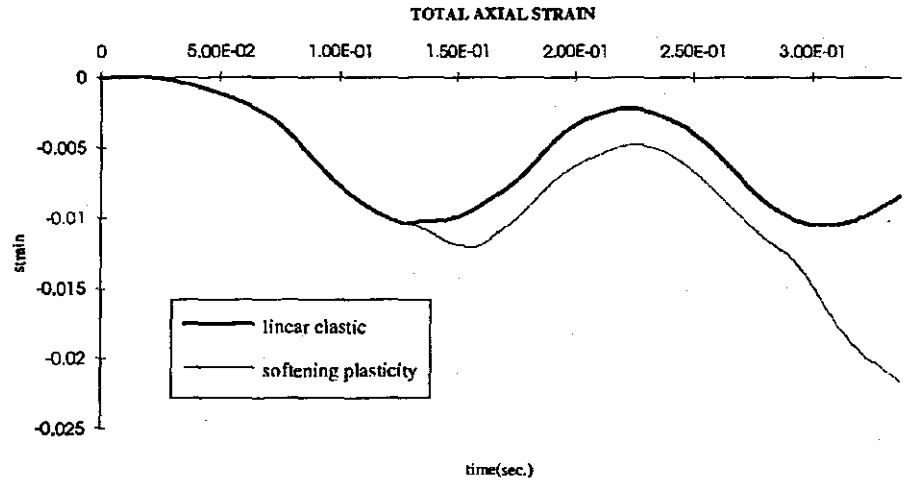

FIG. 5. Comparison between total axial strains vs. time in a Gauss point close to the centre, in the linear elastic case and in plasticity with softening.

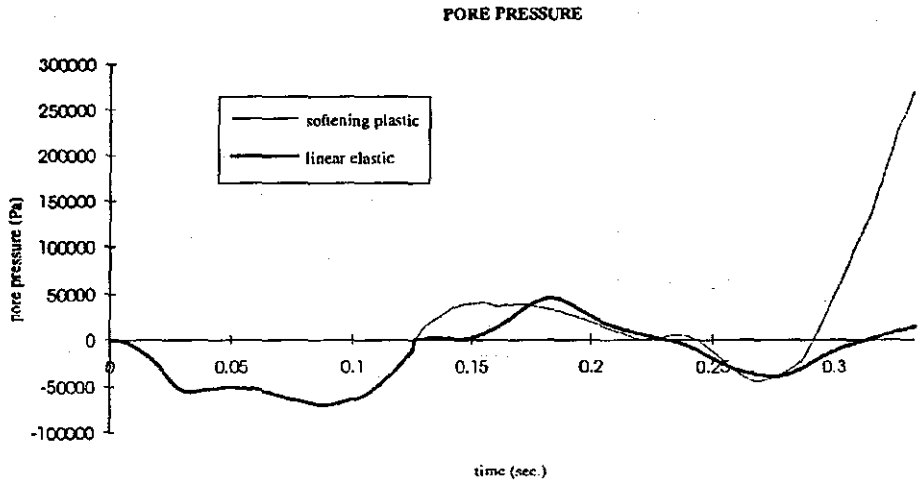

FIG. 6. Comparison between pressures vs. time in the central node in the linear elastic case and in plasticity with softening.

The time transients of strains (Fig. 5) and pressures (Fig. 6) are characterized by a wave form, with a marked regularity up to the onset of the shear band formation ($t < 0.3$ s), since the plastic effect is yet limited. Plastic strain shows a different pattern, characterized by a plateau (Fig. 7). For $t > 0.3$ s loss of periodicity can be noted in Fig. 5, as well as a sudden development of pore water tractions (Fig. 6).

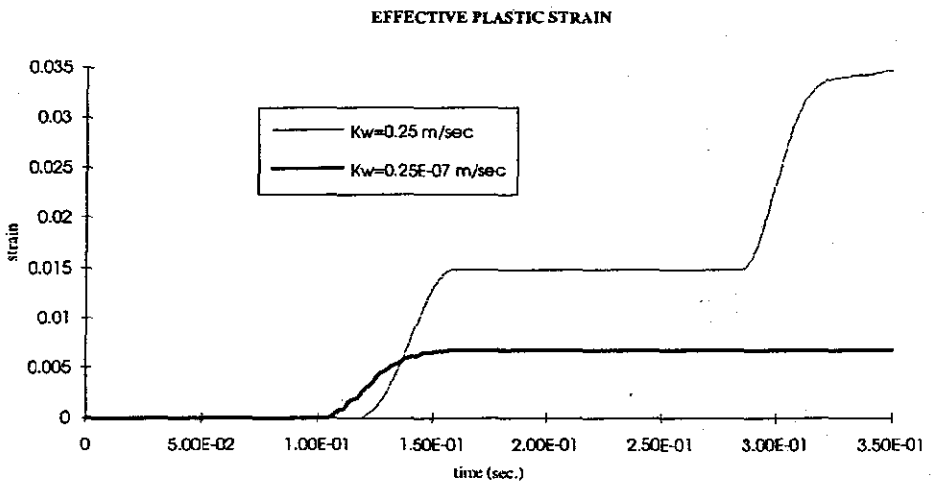

FIG. 7. Comparison between effective plastic strains vs. time in a Gauss point nearest the centre, for different permeabilities.

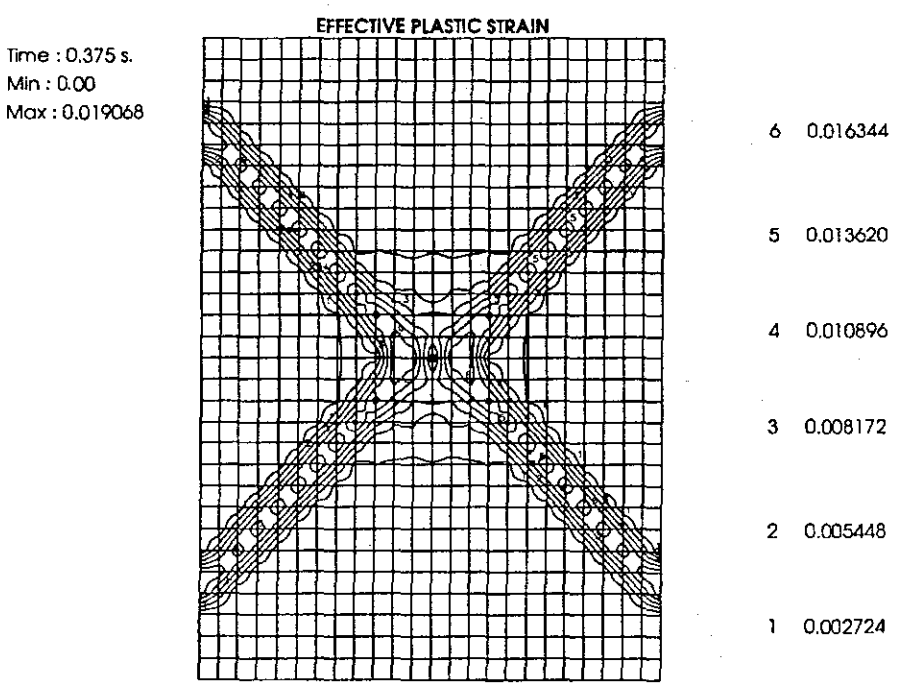

FIG. 8. Effective plastic strains at $t = 0.375\,\mathrm{s}$ with a permeability of $0.25E - 03\,\mathrm{m/s}$.

It should be noted that the material properties for the Mohr-Coulomb model chosen are those of a sand which dilates because of shear. The shear band has hence higher porosity, which implies transient flow into it. In the example, water cannot flow fast enough, hence pore water traction develops in the shear band as can be clearly seen in Figs. 6 and 10.

4.2. Influence of permeability

The permeability affects the degree of coupling between the two phases and presents a significant role in the development of localization. The lower is its value, the higher is the part of the load increment assumed by water and the slower is the transfer to the solid skeleton. Hence coupling effects increase as the permeability decreases.

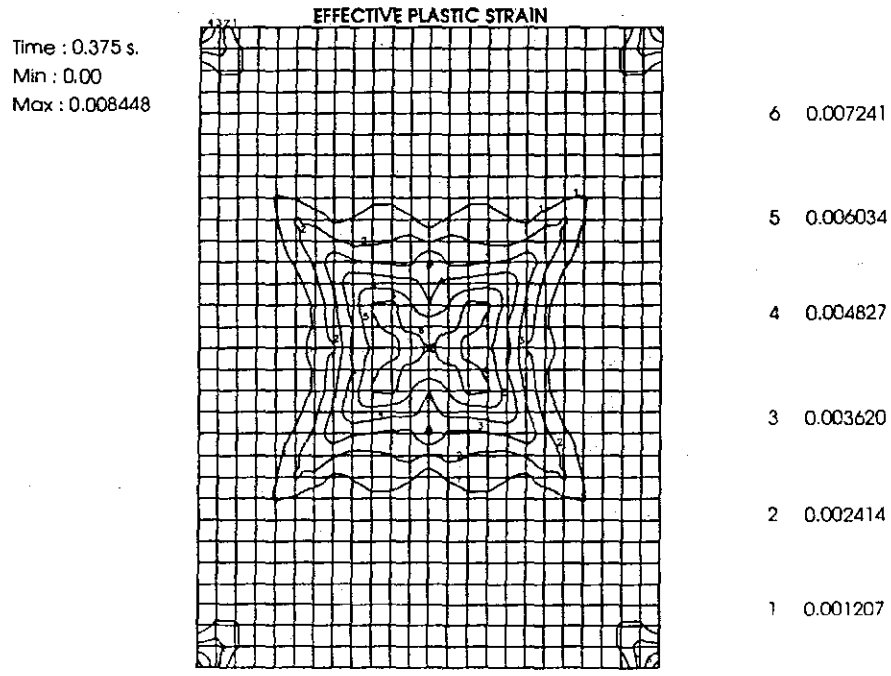

FIG. 9. Effective plastic strains at $t = 0.375$ s with a permeability of $0.25E-10$ m/s.

In localization this implies the variation of the plastic strain levels (Fig. 7), the change of band dimension (compare Figs. 2 and 8) up to the disappearance of their formation (Fig. 9). For a permeability of $0.25E-03$ m/s, pore water pressure localization develops as shown in Fig. 10. As noted previously, we have pore water tractions in the shear band. For a permeability value of 0.25 m/s, no such pore pressure localization has been observed.

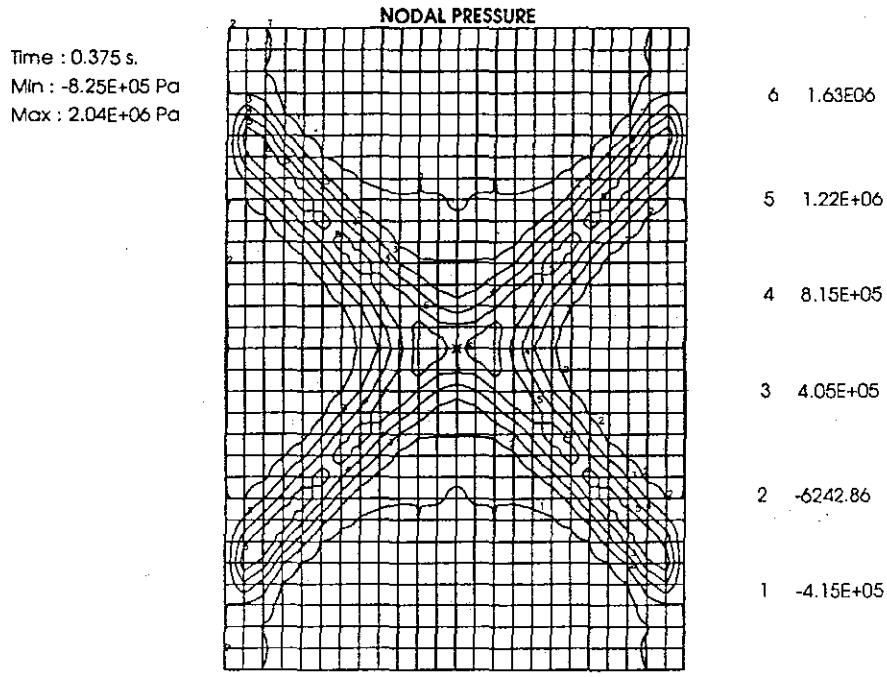

FIG. 10. Nodal pressures at $t = 0.375$ s with a permeability of $0.25E - 03$ m/s.

4.3. Dependence on spatial discretization

Using in a single phase material a rate or gradient-independent material model, the localization is strongly dependent on the chosen discretization, and the numerical solution cannot have a physical meaning. This is connected with the presence of a softening branch in the constitutive relationship, responsible for the loss of hyperbolicity in the equations of motion. The wave propagation disappears because either a wave with zero velocity or two waves with imaginary velocities (stationary jump) appear. Such statement can be easily demonstrated in the one-dimensional case, where the wave velocity is equal to $\pm\sqrt{D_{\mathrm{ep}}/\varrho}$, D_{ep} being the elastoplastic modulus (negative in the softening branch). Hence the system of differential equations becomes ill-posed, i.e. is strongly dependent on the initial and boundary conditions. The absence of a scale parameter in the constitutive law leads to the dependence of the band width on the element dimension. Such an internal length scale may be introduced either by using a model with polar constituents, see e.g. PASTOR *et al.* [15], gradient-dependent plasticity [6] or rate-dependent plasticity.

The tests carried out with program Swandyne [23, 12] have shown that for a multiphase material the situation is not so dramatic, because of the natural presence of a Laplacian (Eqs. (2.10) and (2.18)). The use of rate-dependent plasticity,

e.g. of the model of Duvaut–Lions [5], improves the performance only slightly. This topic will however be further pursued.

5. Conclusions

This paper shows early results of a research in progress on localization in two or three-phase geomaterials. The possibility of initiation of shear band formation using ramp loading has been shown in fully saturated conditions. The influence of permeability on shear band formation has been investigated in some detail. Many questions are still open, especially as far as partially saturated conditions are concerned. The numerical tool presented in this paper is however a good starting point to solve these problems with some degree of confidence.

Acknowledgements

This work has been carried out within the framework of HCM project "ALERT geomaterials" and was partly financed by the Italian Ministry of Scientific and Technological Research (MURST 40%).

Appendix

$$\text{coupling matrix} \quad \mathbf{Q} = \int_V \mathbf{B}_o^T S \mathbf{m} \mathbf{N}_p \, dV,$$

$$\text{mass matrix} \quad \mathbf{M} = \int_V \mathbf{N}_u^T [\varrho_s (1-\phi) + \varrho_l \phi S] \mathbf{N}_u \, dV,$$

$$\text{permeability matrix} \quad \mathbf{H} = \int_V (\nabla \mathbf{N}_p)^T \mathbf{k}_l \nabla \mathbf{N}_p \, dV,$$

$$\text{dynamic seepage matrix} \quad \mathbf{G} = \int_V (\nabla \mathbf{N}_p)^T \mathbf{k}_l \varrho_l \mathbf{N}_u \, dV,$$

$$\text{compressibility matrix} \quad \mathbf{S} = \int_V \mathbf{N}_p^T \frac{1}{Q} \mathbf{N}_p \, dV,$$

$$\text{external load vector} \quad \mathbf{f}^u = \int_V \mathbf{N}_u^T [\varrho_s (1-\phi) + \varrho_l \phi S] \mathbf{b} \, dV + \int_A \mathbf{N}_u^T \mathbf{t} \, dA,$$

$$\text{flow vector} \quad \mathbf{f}^p = \int_V (\nabla \mathbf{N}_p)^T \mathbf{k}_l \varrho_l \mathbf{b} \, dV - \int_A \mathbf{N}_p^T \mathbf{q}^T \mathbf{n} \, dA,$$

$$\text{equivalent force vector} \quad \mathbf{P} = \int_V \mathbf{B}_o^T \sigma'' \, dV,$$

$$\mathbf{F}^u_{n+1} = \mathbf{f}^u_{n+1} - \mathbf{M}_{n+1}\,\ddot{\bar{\mathbf{u}}}_n + \mathbf{Q}_{n+1}\left(\bar{\mathbf{p}}_n + \Delta t\,\dot{\bar{\mathbf{p}}}\right),$$

$$\mathbf{F}^p_{n+1} = \mathbf{f}^p_{n+1} - \mathbf{Q}^T_{n+1}\left(\dot{\bar{\mathbf{u}}}_n + \Delta t\,\ddot{\bar{\mathbf{u}}}_n\right) - \mathbf{H}_{n+1}\left(\bar{\mathbf{p}}_n + \Delta t\Delta\,\dot{\bar{\mathbf{p}}}_n\right) - \mathbf{S}_{n+1}\,\dot{\bar{\mathbf{p}}}_n,$$

$$C_{ll} = \frac{(\alpha-\phi)}{K_s}S^2 + \frac{\phi S}{K_l},$$

$$C_{lg} = \frac{(\alpha-\phi)}{K_s}S(1-S),$$

$$C_{gg} = \frac{(\alpha-\phi)}{K_s}(1-S)^2 + \frac{\phi(1-S)}{K_g},$$

$$\frac{1}{Q} = C_{ll} + \frac{C_{lg}}{S_g}\frac{C_s}{\phi}p_l + C_s = C_s + \frac{\phi S}{K_l} + \frac{(\alpha-\phi)}{K_s}S\left(S + \frac{C_s}{\phi}p_l\right),$$

$$\mathbf{B}^T_{0i} = \begin{bmatrix} \dfrac{\partial N_i}{\partial x_1} & 0 & 0 & 0 & \dfrac{\partial N_i}{\partial x_3} & \dfrac{\partial N_i}{\partial x_2} \\ 0 & \dfrac{\partial N_i}{\partial x_2} & 0 & \dfrac{\partial N_i}{\partial x_3} & 0 & \dfrac{\partial N_i}{\partial x_1} \\ 0 & 0 & \dfrac{\partial N_i}{\partial x_3} & \dfrac{\partial N_i}{\partial x_2} & \dfrac{\partial N_i}{\partial x_1} & 0 \end{bmatrix},$$

$$\mathbf{G}^T_r = \left(\frac{\partial N_i}{\partial x_1}\mathbf{I}, \frac{\partial N_i}{\partial x_2}\mathbf{I}, \frac{\partial N_i}{\partial x_3}\mathbf{I},\right),$$

$$\hat{\sigma} = \begin{pmatrix} \hat{\sigma}_{11} & \hat{\sigma}_{12} & \hat{\sigma}_{13} \\ \hat{\sigma}_{21} & \hat{\sigma}_{22} & \hat{\sigma}_{23} \\ \hat{\sigma}_{31} & \hat{\sigma}_{32} & \hat{\sigma}_{33} \end{pmatrix} \qquad \text{with} \quad \hat{\sigma}_{ij} = \sigma_{ij}\mathbf{I},$$

$$\sigma_{d2} = \begin{pmatrix} \sigma_{11} & \sigma_{11} & \sigma_{11} & 0 & 0 & 0 \\ \sigma_{22} & \sigma_{22} & \sigma_{22} & 0 & 0 & 0 \\ \sigma_{33} & \sigma_{33} & \sigma_{33} & 0 & 0 & 0 \\ \sigma_{23} & \sigma_{23} & \sigma_{23} & 0 & 0 & 0 \\ \sigma_{13} & \sigma_{13} & \sigma_{13} & 0 & 0 & 0 \\ \sigma_{12} & \sigma_{12} & \sigma_{12} & 0 & 0 & 0 \end{pmatrix},$$

$$\sigma_{d1} = \begin{pmatrix} 2\sigma_{11} & 0 & 0 & 0 & \sigma_{13} & \sigma_{12} \\ 0 & 2\sigma_{22} & 0 & \sigma_{23} & 0 & \sigma_{21} \\ 0 & 0 & 2\sigma_{33} & \sigma_{32} & \sigma_{31} & 0 \\ 0 & \sigma_{32} & \sigma_{23} & \overline{\overline{\sigma}}_{23} & \sigma_{21} & \sigma_{31} \\ \sigma_{31} & 0 & \sigma_{13} & \sigma_{12} & \overline{\overline{\sigma}}_{13} & \sigma_{32} \\ \sigma_{21} & \sigma_{12} & 0 & \sigma_{13} & \sigma_{23} & \overline{\overline{\sigma}}_{12} \end{pmatrix} \qquad \text{with} \quad \overline{\overline{\sigma}}_{ij} = \frac{\sigma_{ij} - \sigma_{ji}}{2}.$$

References

1. N. BICANIC and A. SELMAN, *On mesh dependence of failure mode predictions for strain softening analyses*, 1993 [in press].
2. P.J. CHEN, *Growth and decay of waves in solids*, Mechanics of Solids, vol. III, C. TRUESDELL [Ed.], Springer-Verlag, Berlin, Heidelberg 1973.
3. O. COUSSY, *Mécanique des milieux poreux*, Editions Technip, Paris 1991.
4. J.K. DIENES, *On the analysis of rotation and stress rate in deforming bodies*, Acta Mech., **32**, 217–232, 1979.
5. G. DUVAUT and J.L. LIONS, *Les inéquations en mécanique et en physique*, Dunod, Paris 1972.
6. W. EHLERS, *Toward finite theories of liquid-saturated elasto-plastic porous media*, Int. J. Plasticity, **7**, 433–475, 1991.
7. M. HASSANIZADEH and W.G. GRAY, *General conservation equations for multi-phase system. 1. Averaging technique*, Adv. Water Res., **2**, 131–144, 1979.
8. M. HASSANIZADEH and W.G GRAY, *General conservation equations for multi-phase system. 2. Mass, momenta, energy and entropy equations*, Adv. Water Res., **2**, 191–201, 1979.
9. M. HASSANIZADEH and W.G. GRAY, *General conservation equations for multi-phase system. 3. Constitutive theory for porous media flow*, Adv. Water Res., **3**, 25–40, 1980.
10. B. LORET and J.H. PREVOST, *Dynamic strain localization in fluid-saturated porous media*, J. Engng. Mech., **11**, 907–922, 1991.
11. J.E. MARSDEN and T.J.R. HUGHES, *Mathematical foundation of elasticity*, Prentice-Hall, Englewood Cliffs, NJ, 1983.
12. E.A. MEROI, B.A. SCHREFLER and O.C. ZIENKIEWICZ, *Large strain static and dynamic semisaturated soil behaviour*, Int. J. Num. Anal. Meth. Geomech., **19**, 2, 81–106, 1995.
13. F. MOLENKAMP, *Limits to the Jaumann stress rate*, Int. J. Num. Anal. Meth. Geomech., **10**, 151–176, 1986.
14. D.R.I. OWEN, E. ONATE and E. HINTON, Proc. of the third International Conf. on Computational Plasticity; Section 3. Localisation and material instabilities, (Barcelona, 6-10 April, 1992), Pineridge Press, Swansea 1992.
15. M. PASTOR, J.P. VILLOTTE, O.C. ZIENKIEWICZ *et al., Numerical analysis of failure and localization in soils*, Euro-Greco project 4, Strains Localization in Geomaterials, 32–38, 1992.
16. J.R. RICE, *On the stability of dilatant hardening for saturated rock masses*, J. Geophys. Res., **80**, 11, 1531–1536, 1975.
17. J.W. RUDNICKI, *Effect of dilatant hardening on the development of concentrated shear-deformation in fissured rock masses*, J. Geophys. Res., **89**, B11, 9259–9270, 1984.
18. B.A. SCHREFLER, L. SIMONI, K. XI and O.C. ZIENKIEWICZ, *Mechanics of partially saturated porous media*, [in:] Num. Meth. and Const. Mod. in Geom., CISM, **311**, C.S. DESAI and G. GIODA [Ed.], Springer-Verlag, Wien, New York 1993.
19. L.J. SLUYS, *Wave propagation, localization and dispersion in softening solids*, Ph.D. Thesis, Civil Engineering Department of Delft University of Technology, 1992.
20. C. TRUESDELL and W. NOLL, *The non-linear field theories of mechanics*, S. FLÜGGE [Ed.], Handbuch der Physik, vol. III/3, Springer-Verlag, Berlin 1965.
21. C. TRUESDELL and R. TOUPIN, *The classical field theories*, Handbuch der Physik, vol. III/1, Springer-Verlag, Berlin 1960.
22. I. VARDOULAKIS, *Dynamic stability analysis of undrained simple shear on water-saturated granular soils*, Int. J. Numer. Anal. Meth. Geomech., **10**, 2, 177–190, 1986.

23. Y.M. XIE, *Finite element solution and adaptive analysis for static and dynamic problems of saturated-unsaturated porous media*, Ph.D. thesis, Department of Civil Engineering, Swansea University, U.K. 1990.

24. O.C. ZIENKIEWICZ, A..C. CHAN, M. PASTOR, D.K. PAUL and T. SHIOMI, *Static and dynamic behaviour of soils: a rational approach to quantitative solutions. I. Fully saturated problems*, Proc. R. Soc. Lond., A 429, 285–309, 1990.

25. O.C. ZIENKIEWICZ and T. SHIOMI, *Dynamic behavior of saturated porous media: the generalised Biot formulation and its numerical solution*, Int. J. Num. Anal. Meth. in Geom., **8**, 71–96, 1984.

26. O.C. ZIENKIEWICZ and R.L. TAYLOR, *The finite element method*, Vol. 2, McGraw-Hill Book Company, London 1991.

UNIVERSITÀ DEGLI STUDI DI PADOVA
FACOLTÀ DI INGEGNERIA
ISTITUTO DI SCIENZA E TECNICA DELLE COSTRUZIONI, PADOVA, ITALY.

Received November 3, 1994.